Fabrication of LIPSS-based metallic polarization gratings

Alejandro SAN BLAS[*1,2], Ainhara RODRIGUEZ[*1,2], Noemi CASQUERO[*1,2], Santiago Miguel OLAIZOLA[*1,2], Miguel MARTINEZ-CALDERON[*1,2] and Mikel GOMEZ-ARANZADI[*1,2]

[*1] *Ceit-IK4, Spain*
[*2] *Universidad de Navarra, Tecnun, Spain*

Main author's e-mail address: mgomez@ceit.es

Birefringence induced by nanoripples generated by laser (Laser Induced Periodic Surface Structures, LIPSS), enables their use as polarization gratings. Their fabrication is simple, as LIPSS geometry is defined by the characteristics of the laser and the substrate in a one-step process. In this work LIPPS generated on stainless steel have been used to measure the change in polarization of the light reflected on them. Parameters such as period, depth or width of the ripples define the optical properties of these polarization gratings. As the fabrication parameters change, results show a gradual change in polarization. Our experiments, performed with a setup based in cylindrical focusing lens, demonstrate the fast fabrication of samples for different applications, such as waveplates.

Keywords: LIPSS, femtosecond, nanostructures, polarization, waveplate

1. Introduction

The control of polarization is one of the main features in experimental setups where optic and photonic properties are studied. To perform this control, one of the most used elements are waveplates. Waveplates introduce a fixed phase delay between the orthogonal components of the electric field, and this way a change in the polarization of the incident beam can be achieved. In most cases, the waveplates used are transmittive. For this type of waveplates birefringent materials are used, and the thickness is used in order to tune their properties. However, there are some cases in which the temporal dispersion must be kept below one specific value, or the damage threshold exceeds that of the materials commonly used for the transmittive waveplates (i.e. crystals). In this cases, reflective waveplates are used instead. This type of waveplates are readily available and are based in periodic gratings. The gratings are fabricated using lithography or laser interference methods [1], but present some disadvantages. To mention a few, the processes tend to be time consuming, additives are used that present a risk for the environment, and most of the time the available range of grating period offered by the manufacturer is considerably narrow.

As an alternative to these manufacturing methods, laser technology is a method for the production of nanostructures widely reported in bibliography. The first Laser-Induced Periodic Surface Structures (LIPSS) were obtained in 1965. LIPSS have a period in the order of the wavelength of the incident light, and they appear in a wide range of materials when irradiated with a laser source. Their main properties, specifically the period and height, can be controlled with the parameters of the incident laser light: fluence, wavelength and pulse duration [2]. LIPSS have been widely used for surface functionalization, which provides different properties to the final device. Some examples of this include the fabrication of hydrophilic/phobic surfaces [3], mechanical stress detection [4] or fine tuning of the color of the surface by the variation of LIPSS geometry [5]. However, to the best of our knowledge, they have not been applied as gratings for reflective waveplates. A waveplate, as stated before, is an element that introduces a phase displacement between the orthogonal components of the incident light, which in turn produces a change in its polarization state [6].

In the present work, the fabrication of reflective waveplates using femtosecond laser technology is reported. The main feature of our setup is the use of a cylindrical lens which, when used to focus the laser beam onto stainless steel samples, enables the generation of LIPSS on their surface on a broad front, making this a fast, one-step fabrication method. As a second interesting feature, the control of the properties of the waveplate by the tuning of the fabrication parameters is demonstrated.

2. Materials and methods

2.1 Laser setup

A Ti:Sapphire laser was used to irradiate the stainless steel samples in order to create LIPSS on its surface. The laser system produces 120 fs pulses with a central wavelength of 800 nm and repetition rate of 1 kHz. The pulse energy is adjusted in this system with a variable attenuator consisting of a half-wave plate and a polarizer. A motorized half-wave plate enables the rotation of the polarization of the laser beam. A combination of a cylindrical lens with a focal of 100 mm and a spherical lens with a focal of 75 mm is used to focus the beam on the sample. The beam profile obtained with this setup is a line perpendicular to the X-axis, which will form the front from where the LIPSS will be created. A CMOS camera was used to monitor the process, and a white LED was added in order to illuminate, as shown in Fig 1. The sample was displaced below the beam line using XZ motorized stages, controlling both the pro-

cessing speed and the line size projected by the cylindrical and spherical lenses.

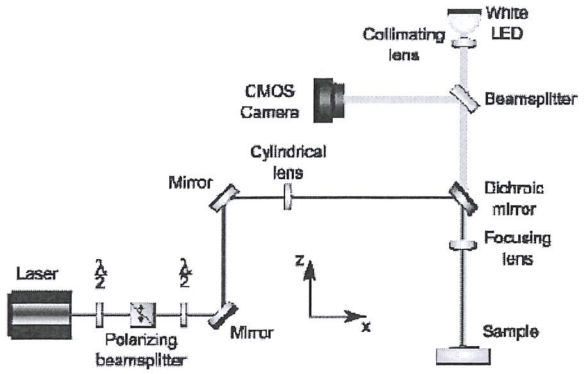

Fig. 1 Setup used in the processing of the samples.

2.2 Fabrication process

The material used as a substrate for the generation of LIPSS consisted in stainless steel samples of dimensions 10 mm x 20 mm. In order to remove any particles present on the surface before the process, or particles generated during the process itself, the samples were immersed in an acetone bath and stirred in an ultrasound generator.

The process to generate the LIPPS on the surface of the samples followed always the same procedure. The sample was moved under the laser beam at a constant speed along the X-axis, and this value changed from sample to sample. The range of speeds used for the different samples varied between 0.8 and 2.4 mm/s. In the case of the position of the Z-axis, it was adjusted so that the width of the laser beam projected onto the sample was 30 μm. The energy was kept constant at a value of 1.4 mJ for all the processed samples. In order to obtain LIPSS perpendicular to the advance of the beam front, the polarization of the laser light was set parallel to the motion of the X-axis.

2.3 Characterization

A He-Ne laser (633 nm wavelength) was used to irradiate the samples at an angle of 5° with respect to the surface normal, and a polarimeter (Thorlabs PAX1000IR1) was used in order to measure the effect of the generated LIPSS on the polarization. The polarization of this incident laser light was controlled with a half wave plate. With the aim of detecting birefringence in a more efficient way, the polarization of the incident beam was set to 45° (linear polarization) with respect to the orientation of the LIPSS. The specular reflection of light was analyzed with the polarimeter.

The topology of the features generated on the surface of the samples was characterized with SEM (Scanning Electron Microscope), and 2D-FFT (two-dimensional Fast Fourier Transform) was performed to the images obtained in electron microscopy to measure the period of the generated LIPSS. This was done because the relation between the period of the LIPSS (Λ) and the distance between FFT peaks (d) is given by the equation Λ=2/d. Atomic Force Microscopy (AFM) was used to measure the height of the LIPSS. In order to do so, sweeps were performed in large areas of 30 μm x 30 μm, which allowed obtaining an average value quite accurately. This was done by measuring the vertical distance between positive and negative peaks, and averaging them to obtain the average height of the sample. Images of the transversal profile of the LIPSS were obtained through the FIB (Focused Ion Beam) technique implemented in a SEM microscope.

3. Results and discussion

Results obtained by the polarimeter show that, varying the processing speed, the ellipticity of the beam polarization can be modified (Fig. 2). As observed in the left part of the graph, an increase of the processing speed from a minimum of 0.8 mm/s to 1.6 mm/s results in an increase in the ellipticity from 2.91° to 11.04°. Above a processing speed of 1.6 mm/s the trend reverses. This means that as the processing speed increases above 1.6 mm/s, the ellipticity starts to decrease, reaching a value of 1.18° at a speed of 2.4 mm/s. Taking all of this into account, the main conclusion is that a change in the polarization is observed, from linear to elliptical, with a varying degree of ellipticity that changes smoothly with processing speed. At the same time, an effect on the reflectivity is seen. It increases continuously from 2.2% for samples processed at 0.8 mm/s to 13% for samples processed at 2.4 mm/s. In order to understand the effect of the LIPSS on this parameter, it must be said that the reflectivity of an unprocessed stainless steel sample measured from the same polarimeter also at an angle of 5° is 38%.

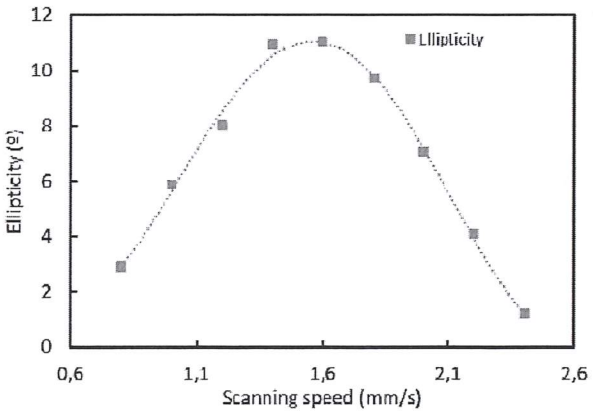

Fig. 2 Ellipticity of the polarization versus the processing speed.

The results show a strong coherence between samples processed with the same parameters. This suggests that the setup used for their fabrication is consistent and robust, once it is assured that the parameters are maintained constant. This is especially true for the laser spot size, as according to our experience a relatively minor variation in this parameter could yield a significant change in the final result. The main difference of this setup and others used for the fabrication of LIPSS is the focal length of the optical devices. Other setups tend to use microscope objectives with short working distances, in the order of the few millimeters. Alternatively, our setup uses long focal lenses and therefore has a long Rayleigh length. This means that in

our setup the positioning of the sample in the Z axis, i.e. the distance between the sample and the lens, is not as critical as in other setups. At the same time, the use of cylindrical lenses in this experiment means that we can program a simpler processing strategy. Since the projected line on the sample is long enough to cover one of the axes, the samples are only displaced along the axis perpendicular to the laser front. As a result, this strategy requires much less processing time and the issues that arise when a lateral overlap is performed are avoided.

Regarding the LIPPS morphology, a study has been carried out using SEM. Both Figs. 3 and 4 show the surface of two samples, corresponding to processing speeds of 0.8 mm/s (Fig. 3) and 1.6 mm/s (Fig. 4). The election of these two samples was motivated for the fact that they represent the lowest (0.8 mm/s) and highest (1.6 mm/s) change in polarization as observed with the polarimeter. Fig. 3 shows that there is a slight difference in the shape of the LIPSS, where the ripples show imperfections along the crest. The observed morphology concords with the results reported in literature, and allows us to conclude that it is caused by the lower processing speed and higher total fluence. Regarding the SEM image displayed in Fig. 4 a better definition of the LIPSS can be appreciated, with a much lower concentration of imperfections. In both cases, the 2D-FFT images show two main peaks in intensity to each side of the origin (which is located in the center of the image). The existence of two peaks instead of a single one means that the generated LIPSS do not conform a perfectly periodic structure. If that was the case, there would be a single point corresponding to a single frequency and orientation. Instead, there is a stronger peak and a weaker one at double frequency, both with some range of frequencies and orientations that vary between samples. These imperfections could be a limiting factor for the fabrication of working gratings, as they could limit their effectiveness. The main effect derived from them would be a reduction in the change of the reflectivity and the ellipticity.

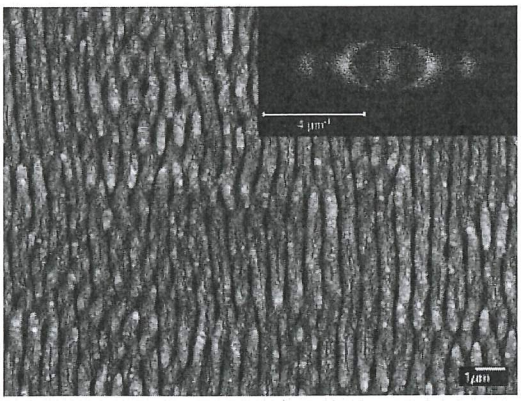

Fig. 3 SEM image of a sample fabricated at 0.8 mm/s. Inset: 2D-FFT of the sample.

In order to obtain the main frequency or period of the LIPSS, a measurement is performed in the 2D-FFT images, calculating the distance from the point of maximum intensity to the origin. The main conclusion from these measurements is that the period of the generated LIPSS increases linearly with the processing speed, from 602 to 651 nm. This is an important outcome, because we expect the period of the LIPSS to be a key factor in the behavior of the grating.

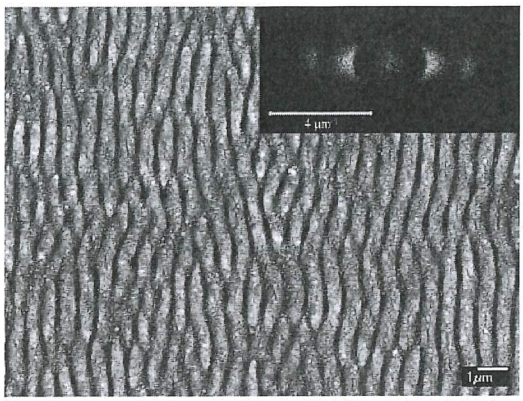

Fig. 4 SEM image of a sample fabricated at 1.6 mm/s. Inset: 2D-FFT of the sample.

Regarding the results obtained with AFM, we have observed that the height measured in the different samples does not vary much. This means that this parameter does not seem to be a factor in the reflective behavior of the LIPSS generated onto the samples, or at least that a change in this behavior can be performed without the need to modify the height. Fig 5 shows an example of FIB profile. The upper layer is the platinum coating deposited onto the sample in order not to affect the sample while performing the trench with the ion beam. The first thing that can be noticed is that the shape of LIPSS is somewhat irregular, and this is the main reason why complementary AFM measurements where performed. Both to cover a larger area, and at the same time to have a larger quantity of values in order to obtain an average value of height as accurate as possible. As a conclusion, it must be said that similar structures and heights were observed between the two methods (AFM and FIB), concluding that both methods are a valid source of data and that the height of the LIPSS is quite regular along the Y axis (perpendicular to the laser front).

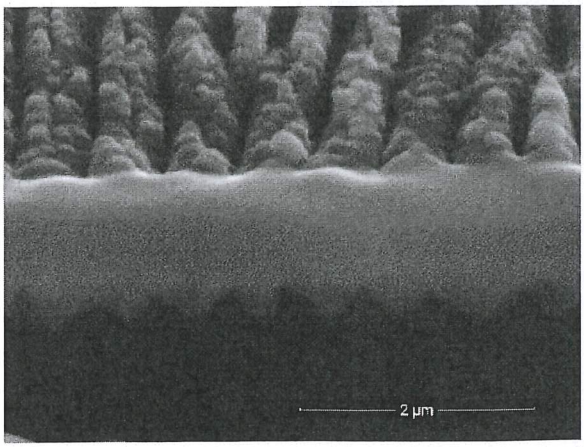

Fig. 5 FIB section of a sample processed at 0.8 mm/s. Structures with different profiles can be seen.

Nevertheless, it must be said that the beam emitted by the laser has a gaussian shape. This means that as a cylindrical lens has been used to change the size of the spot from a circle to a line, the energy transmitted at both ends of the line is logically lower than at the main central section. Therefore, the regularity of the height of the LIPSS can only be assured along the central section swept by the laser. On both ends certain irregularities can be appreciated, including the appearance of double period LIPSS as expected according to bibliography.

4. Conclusion

In this work, we have proven that a setup based on a cylindrical lens can be a powerful tool in order to fabricate LIPSS with a much reduced process time. At the same time, we have shown the potential to use these LIPSS for the fabrication of reflective waveplates. The use of a cylindrical lens with a larger focal length offers two advantages. The aforementioned processing time, that is in the order of 1 mm/s, and a stable and repeatable fabrication process. This second advantage stems from two factors. First, the sample only is displaced along one axis, avoiding possible issues regarding the lateral overlapping and, second, using a longer focal length reduces the positioning error with respect to the distance between the sample surface and the lens.

The maximum change in ellipticity achieved is 11°, although we expect to reach higher values in future experiments that will be performed with the same setup. Regarding the morphology of the LIPSS we have found that, although the exact relation between polarization change and LIPSS morphology is not yet well understood due to the different factors that could affect this change, two are the main factors that we deduce could be it. The first one is the period, and second one is the shape (regularity and homogeneity) of the LIPSS.

Acknowledgments and Appendixes

This work is part of the following projects: ECOGRAB, funded by the Government of Spain under the RETOS COLABORACIÓN I+D+I program and LASER4SURF, that has received funding from the European Union's Horizon 2020 research and innovation program under grant agreement No 768636.

References

[1] N. Passilly, K. Ventola, P. Karvinen, P. Laakkonen, J. Turunen, J. Tervo: Appl. Opt., 46, (2007) 4258-4265.

[2] J. Bonse, S. Höhm, S. V. Kirner, A. Rosenfeld, J. Krüger: IEE Journal of Selected Topics in Quantum Electronics, 23 (3), (2017).

[3] M. Martínez-Calderón, A. Rodríguez, A. Dias-Ponte, M.C. Morant-Miñana, M. Gómez-Aranzadi, S.M. Olaizola: Appl. Surf. Sci., 374, (2016) 81-89.

[4] S. Gräf, C. Kunz, A. Undisz, R. Wonneberger, M. Rettenmayr, F. A. Müller: Appl. Surf. Sci., 471, (2019) 645-651.

[5] B. Dusser, Z. Sagan, H. Soder, N. Faure, J.P. Colombier, M. Jourlin, E. Audouard: Optics Express, 18 (3), (2010) 2913-2924.

[6] C. Oh and M.J. Escuti: Phys. Rev. A, 76 (043815), (2007) 1-8.